New Journal of Physics
The open access journal at the forefront of physics

Deutsche Physikalische Gesellschaft DPG IOP Institute of Physics

PAPER • OPEN ACCESS

Two- and three-terminal far-from-equilibrium thermoelectric nano-devices in the Kondo regime

To cite this article: Ulrich Eckern and Karol I Wysokiski 2020 *New J. Phys.* **22** 013045

New Journal of Physics
The open access journal at the forefront of physics

Deutsche Physikalische Gesellschaft DPG
IOP Institute of Physics

Published in partnership with: Deutsche Physikalische Gesellschaft and the Institute of Physics

OPEN ACCESS

RECEIVED
1 July 2019

REVISED
23 December 2019

ACCEPTED FOR PUBLICATION
7 January 2020

PUBLISHED
23 January 2020

PAPER

Two- and three-terminal far-from-equilibrium thermoelectric nano-devices in the Kondo regime

Ulrich Eckern[1] **and Karol I Wysokiński**[2]

[1] Institute of Physics, University of Augsburg, 86135 Augsburg, Germany
[2] Institute of Physics, M. Curie-Skłodowska University, pl. M. Curie-Skłodowskiej 1, 20-031 Lublin, Poland

E-mail: ulrich.eckern@physik.uni-augsburg.de **and** karol.wysokinski@poczta.umcs.lublin.pl

Keywords: nanodevices, thermoelectricity, far from equilibrium, Kondo effect, nonlinear response

Supplementary material for this article is available online

Abstract

This paper analyses the thermoelectric power of two- and three-terminal quantum dot devices under large thermal ΔT and voltage V biases, and their performance as thermoelectric heat engines. The focus is on the interaction between electrons, far-from-equilibrium conditions, and strongly nonlinear transport, which all are important factors affecting the usefulness of the devices. To properly characterise the thermoelectric properties under such conditions, two different Seebeck coefficients are introduced, generalizing the linear response expression. In agreement with previous work, we find that the efficiency of the three-terminal thermoelectric heat engine, as measured by the delivered power, is optimal far from equilibrium. Moreover, strong Coulomb interactions between electrons on the quantum dot are found to diminish the efficiency at maximum power, and the maximal value of the delivered power, both in the Kondo regime and beyond.

1. Introduction

Thermoelectricity, the invention of the 19th century, is still at the forefront of research due to its importance for space exploration and automotive industry [1], and many more branches of modern technology both at large [2] and small [3] scales. Attempts to find high performance thermoelectric bulk materials [4], including those with topologically non-trivial [5] band structure, have seen limited progress. In the last few decades, a lot of attention has been put forward towards nano-devices [6] and molecular systems [7, 8], utilizing quantum effects to boost their thermoelectric performance towards the thermodynamic limit [9].

When a temperature gradient ∇T (or a temperature difference ΔT) is established across a bulk material, a voltage V is generated. The response of an isotropic system is characterised by the Seebeck coefficient

$$S = -\left(\frac{V}{\Delta T}\right)_{I=0,\Delta T\to 0}, \tag{1}$$

defined under the condition of zero charge current. The same formal definition can be used for a nano-structure with two external electrodes [10] (see figure 1(a)). However, equation (1) has to be generalized for geometries with several electrodes—as, e.g. the one shown in figure 1(b)—where a whole matrix of Seebeck coefficients [11, 12] has to be introduced.

In bulk systems the linear approximation is generally a valid simplification. Under such a condition the thermoelectric figure of merit, $ZT = GS^2\mathrm{T}/\kappa$, where G is the conductance, and κ the thermal conductance, is viewed as the most important factor deciding on the usefulness of the material as heat to electricity converter: namely, the efficiency is given by $\eta = \eta_C(\sqrt{ZT+1}-1)/(\sqrt{ZT+1}+1)$, where η_C is the Carnot value. In nanostructures containing quantum dots, however, we are virtually always dealing with a nonlinear situation, as mentioned earlier [13–15], and carefully discussed recently [6]. The small ratio of the sample length to the thermalization length in nanostructures is responsible for their very different behaviour compared to bulk systems. This has a profound effect on the analysis of small heat engines, and implies that the thermoelectric

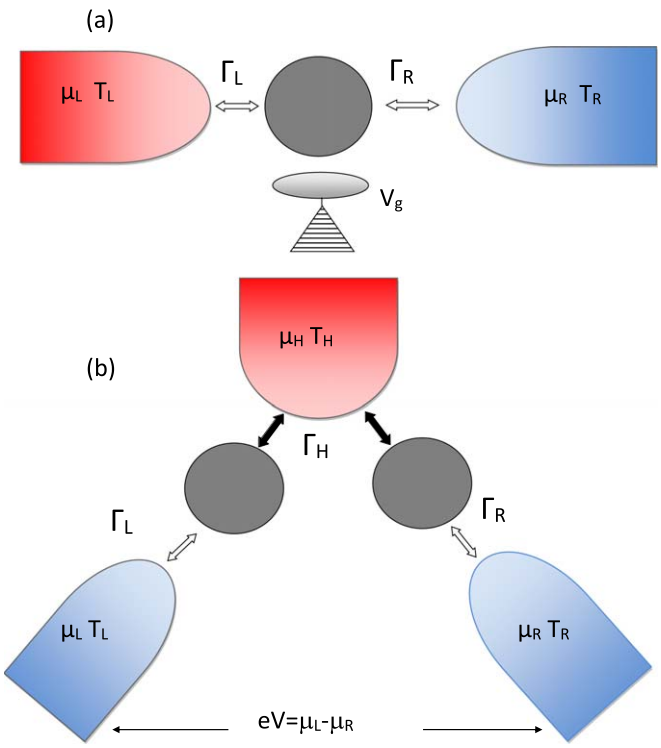

Figure 1. Two examples of devices with quantum dots. In panel (a) we show a two-terminal quantum dot device with the left electrode at higher temperature (red). Panel (b) shows a simple nano-engine with one hot (red) and two cold electrodes (blue) and two quantum dots (grey). In the latter case the filtering properties of quantum dots are important for the performance of the device.

figure of merit ZT is not a useful parameter anymore to judge the efficiency. In particular, a nano-system with a large ZT [16] may in fact feature a small efficiency [17, 18].

From a basic point of view, the Seebeck coefficient provides additional and novel information about the studied system compared to that obtained from the electrical conductivity: the latter 'measures', in the simplest case, the density of states at the Fermi level, $N(E_F)$, and the former its slope, $N'(E_F)$. The thermopower can also be related to the entropy flowing between different parts of the system. In fact, the entropy of nano-systems has been recently measured [19] by means of thermoelectric transport. A strong increase of S in nano-devices and nano-structured materials has been observed [20], in agreement with the earlier proposal [21]. Recent studies [22] have shown that doping or nano-structuring bulk thermoelectric materials may lead to the required modifications of the energy spectrum close to E_F, but also to a localization of states which deteriorates the system's performance.

Furthermore, it has been proposed [14, 23] that nonlinear working conditions can favourably affect the performance of heat engines. Recent studies in this direction include [24–29] and have been reviewed recently [30].

The aim of the present work is to study the thermoelectric transport of quantum dot based nano-devices by means of the non-equilibrium Green function approach, taking Coulomb interactions and nonlinear effects into account. In the nonlinear regime, more general definitions of the Seebeck coefficient than that given in equation (1) are needed; these are especially important when an externally applied voltage V is present while the system is thermally biased. In the presence of interaction and at low temperature, the Kondo effect is expected to dominate the transport properties [31–36]. The present investigation, which significantly extends our previous studies of non-equilibrium screening effects [37] in three-terminal two-quantum-dot heat engines [28, 38], is important for a better understanding of the interaction effects in far-from-equilibrium situations and in the Kondo regime.

As the theoretical treatment of an interacting quantum dot out-of-equilibrium is of importance in itself, we present in some detail the semi-analytical technique proposed by Lavagna [39]. It is based on the equation of motion method (EOM) [40] for the non-equilibrium (or Keldysh) Green functions [41], with important additions introduced by her which allow to properly describe the Kondo effect in the linear and the nonlinear regime, i.e. under large voltage and temperature differences between the electrodes, as well as for the particle-hole symmetric model. We shall discuss this in more detail at the end of the next section.

The use of the equation of motion (EOM) technique for studying the single-impurity Anderson model has a long history [42–44], mainly in the context of impurities in metals. Some of the attempts at generalizing the original EOM and the decoupling procedures have been summarized in [45].

The organization of the paper is as follows. In section 2 we present the model and our approach of calculating the charge and heat currents by means of the Keldysh non-equilibrium Green function (GF) technique. We also derive the exact—in the wide-band-limit—formula for the lesser GF. The resulting spectral function of the quantum dot is discussed in section 3 at low temperatures and for various conditions including particle-hole symmetry and non-equilibrium. Two relevant definitions of the Seebeck coefficients, valid in the nonlinear regime, are proposed and evaluated in section 4. The Coulomb interaction between electrons in the three-terminal quantum dot heat engine is found to diminish the performance of the device in question, as discussed in section 5. The Kondo effect shows up as a two-leaf structure of the performance diagram on the efficiency-power plane. Summary and conclusions are given in section 6.

2. Modelling the device and calculating currents

Here we discuss the simple geometry where the system consists of a quantum dot(s) tunnel-coupled to two (three) normal electrodes as shown in figure 1. The Hamiltonian of the system is written as

$$H = \sum_{\lambda,k,\sigma} \varepsilon_{\lambda k} n_{\lambda k\sigma} + \sum_{\sigma} \varepsilon_\sigma n_\sigma + U n_\uparrow n_\downarrow + \sum_{\lambda k\sigma} (V_{\lambda k\sigma} c^\dagger_{\lambda k\sigma} d_\sigma + V^*_{\lambda k\sigma} d^\dagger_\sigma c_{\lambda k\sigma}), \tag{2}$$

where $n_{\lambda k\sigma} = c^\dagger_{\lambda k\sigma} c_{\lambda k\sigma}$ and $n_\sigma = d^\dagger_\sigma d_\sigma$ denote particle number operators for the leads and the dot, respectively. The operators $c^\dagger_{\lambda k\sigma}(d^\dagger_\sigma)$ create electrons in respective states $\lambda k\sigma\,(\sigma)$ in the leads $\lambda = L, R, H$ (on the dot). The wave vector k denotes the Bloch state in the electrodes, the spin is $\sigma = \pm 1$ ($\uparrow$, $\downarrow$), and ε_σ is the generally spin-dependent dot electron energy level. For the concrete results presented in the next sections we will take ε_σ to be spin-independent, $\varepsilon_\uparrow = \varepsilon_\downarrow = \varepsilon_d$. The quantity $V_{\lambda k\sigma}$ describes the tunneling of electrons from the dot to the electrode λ, and the Hubbard parameter U the repulsion between two electrons on the dot.

Calculations of the charge and heat currents flowing out of a given lead are standard [41]. Evaluating the required commutators one arrives at the expressions

$$I_\lambda = \frac{ie}{\hbar} \int \frac{dE}{2\pi} \sum_\sigma \Gamma^\lambda_\sigma(E) \{G^<_\sigma(E) + f_\lambda(E)[G^r_\sigma(E) - G^a_\sigma(E)]\}, \tag{3}$$

$$J_\lambda = \frac{ie}{\hbar} \int \frac{dE}{2\pi} \sum_\sigma \Gamma^\lambda_\sigma(E)(E - \mu_\lambda) \{G^<_\sigma(E) + f_\lambda(E)[G^r_\sigma(E) - G^a_\sigma(E)]\}. \tag{4}$$

The parameters $\Gamma^\lambda_\sigma(E) = 2\pi \sum_k |V_{\lambda k\sigma}|^2 \delta(E - \varepsilon_{\lambda k})$ describe the coupling between the dot and the respective electrodes. The Green functions $G^i_\sigma(E) = \langle\langle d_\sigma | d^\dagger_\sigma \rangle\rangle^i_E$ with $i = r, a, <$ determine the spectral properties of the quantum dot as well as the transport properties of the whole system. Having in mind non-equilibrium transport induced by a voltage bias and/or a temperature difference, we keep the dependence of the Fermi distribution functions $f_\lambda(E)$ on the electrode λ via its chemical potential μ_λ and its temperature T_λ.

The important issue is the calculation of the lesser GF entering the above equations. In the literature various approximate schemes are used. Here, we show that in the steady state and in the wide-band approximation (i.e. for energy independent couplings: $\Gamma^{L,R}_\sigma(E) = \Gamma^{L,R}_\sigma$), one can derive [39] the *exact* expressions for the lesser GF in terms of the retarded and advanced functions and thus closed formulas for the currents. First, from $\langle n_\sigma \rangle = \langle c^\dagger_\sigma(t) c_\sigma(t) \rangle$ and the definition of the lesser GF, one has [41]

$$\langle n_\sigma \rangle = -i \int \frac{dE}{2\pi} G^<_\sigma(E). \tag{5}$$

The derivation then makes use of the fact that in the steady state

$$0 = \frac{d\langle n_\sigma \rangle}{dt} = \left\langle \frac{dn_\sigma}{dt} \right\rangle = -\left\langle \frac{i}{\hbar}[n_\sigma, H] \right\rangle. \tag{6}$$

Working out the commutator in (6), using (5) and the Langreth theorem [46], it is straightforward to derive the following 'self-consistency' condition [39]:

$$\langle n_\sigma \rangle = i \int \frac{dE}{2\pi} \frac{\Gamma^L_\sigma f_L(E) + \Gamma^R_\sigma f_R(E)}{\Gamma^L_\sigma + \Gamma^R_\sigma} [G^r_\sigma(E) - G^a_\sigma(E)]. \tag{7}$$

Let us underline again that the expression (7) is exact under the proviso that the couplings to the leads are energy independent, $\Gamma^\lambda_\sigma(E) \equiv \Gamma^\lambda_\sigma = \text{const}$. If this condition is violated, as it might be the case in graphene [47–49], hybrid systems with one (or both) of the electrodes being a superconductor, e.g. d-wave [50], other approaches are needed. For models with energy dependent couplings one still has to rely on approximate relations between the lesser self-energy $\Sigma^<_\sigma(E)$ and the retarded one, $\Sigma^r_\sigma(E)$, making use of Ng's approximation [51], a

generalisation of the fluctuation-dissipation theorem [24], or using the equation of motion for the lesser GF [52] and suitable decoupling. For recent attempts to include the energy-dependent couplings, see the paper [53].

Within the above (exact in the steady state and for constant Γ's) formulation, the charge current across the two-terminal system can be written in terms of the retarded GF only:

$$I = \frac{2e}{\hbar}\sum_{\sigma}\tilde{\Gamma}_{\sigma}\int\frac{\mathrm{d}E}{2\pi}[f_L(E) - f_R(E)]\,\mathrm{Im}\,G^r_{\sigma}(E), \tag{8}$$

where $\tilde{\Gamma}_{\sigma} = \Gamma^L_{\sigma}\Gamma^R_{\sigma}/(\Gamma^L_{\sigma} + \Gamma^R_{\sigma})$. We stress that the above formula is an exact representation of the current in terms of the retarded GF of the interacting Hamiltonian, which has to be calculated either numerically or analytically. Here we adopt the latter approach, though obviously calculating the GF analytically requires some approximations; see the supplementary material[3] for details. In brief, the decouplings we are using ensure that the GFs are formally exact up to second order in the couplings. Additionally, we correct the result by phenomenologically introducing the lifetimes [39] of various states, which is important to capture the Kondo effect. It turns out that the proposed scheme properly describes the Kondo resonance in the density of states even in the particle-hole symmetric model. The expression (8) is analogous to the well-known Meir–Wingreen formula [54]. One finds $I = I_L = -I_R$ for the charge current, and $\dot{Q} = J_L + J_R$ for the total heat current leaving the leads. For later use we define the power, $P = (\mu_R - \mu_L)I/e$, and the voltage bias, $V = (\mu_R - \mu_L)/e$, across the system.

Our general formulas for the charge and heat currents (4) are readily applied, e.g. to the three-terminal system shown in figure 1(b). In such a device, the heat is flowing from the hot to the two cold electrodes. We assume that no charge current flows out of or into the hot electrode. The charge flow is controlled by the gate bias of the quantum dots, which hence act as energy filters. The total heat current in the system is

$$J = J_H + J_L + J_R. \tag{9}$$

Introducing a 'load' between the two cold electrodes, in the figure (1) shown as an external voltage V, one finds the system's energy harvesting efficiency as

$$\eta = \frac{IV}{J_H}. \tag{10}$$

To calculate currents we 'only' require the retarded Green function. There exist a few numerically exact approaches: e.g. among the many techniques applied to study the single-impurity Anderson model the quantum Monte Carlo [55] and the numerical renormalization group [56] methods should be mentioned. However, in this work we will use the analytic EOM technique, which has proven to be quantitatively correct [39, 57], and valid far from equilibrium. In addition, in our opinion this approach is physically more transparent than purely numerical methods, as discussed below.

After a couple of manipulations, the on-dot GF is obtained as follows:

$$\langle\langle d_{\sigma}|d^{\dagger}_{\sigma}\rangle\rangle_E = \frac{1 + I_d(E)[\langle n_{\bar{\sigma}}\rangle + b_{1\bar{\sigma}} - b_{2\bar{\sigma}}]}{E - \varepsilon_{\sigma} - \Sigma_{0\sigma} + I_d(E)[\Sigma^T_1 + \Sigma^T_2 - (b_{1\bar{\sigma}} - b_{2\bar{\sigma}})\Sigma_{0\sigma}]}, \tag{11}$$

where

$$I_d(E) = \frac{U}{E - \varepsilon_{\sigma} - U - \Sigma_{0\sigma} - \Sigma^{(1)}_{\sigma} - \Sigma^{(2)}_{\sigma}}. \tag{12}$$

Details of the derivation and the definitions of the parameters are given in the Supplementary Material (See footnote 3). The above expression for the GF, equation (11), agrees with that obtained earlier by Lavagna [39].

It should be remembered that previous attempts to calculate the on-dot GF by means of the EOM technique encountered a serious problem. Namely, it was not possible to describe the Kondo resonance for the particle-hole symmetric system. Lavagna and co-workers [39, 57], however, have shown that for the correct description of the Kondo effect it is necessary to supplement the equations for the dot GF by two ingredients. First, one should introduce the finite lifetimes of singly and doubly occupied states on the dot. Second, it is important to include the many-body renormalization of the dot energy level ε_d. Thus, first, one replaces the $E + \mathrm{i}0$ terms in the definitions of various Green and correlation functions by $E + \mathrm{i}\tilde{\gamma}_{\alpha}$, where the inverse lifetimes $\tilde{\gamma}_{\alpha}$ of the excited states $\alpha = |\sigma\rangle, |\uparrow,\downarrow\rangle$ are due to higher order processes. They can be calculated up to the desired order via the generalized Fermi rule as

$$\tilde{\gamma}_{\alpha} = 2\pi\sum_{|f\rangle}|\langle T(E_{\alpha})\rangle|^2\delta(E_{\alpha} - E_f), \tag{13}$$

with $T(E) = \hat{V} + \hat{V}g(E)\hat{V} + \cdots$ the scattering matrix, where $\hat{V}$ denotes the part of the Hamiltonian describing the coupling between quantum dot and reservoirs. Second, one replaces ε_d by $\tilde{\varepsilon}_d$, to be calculated self-

[3] Supplementary material, available online at stacks.iop.org/NJP/22/013045/mmedia.

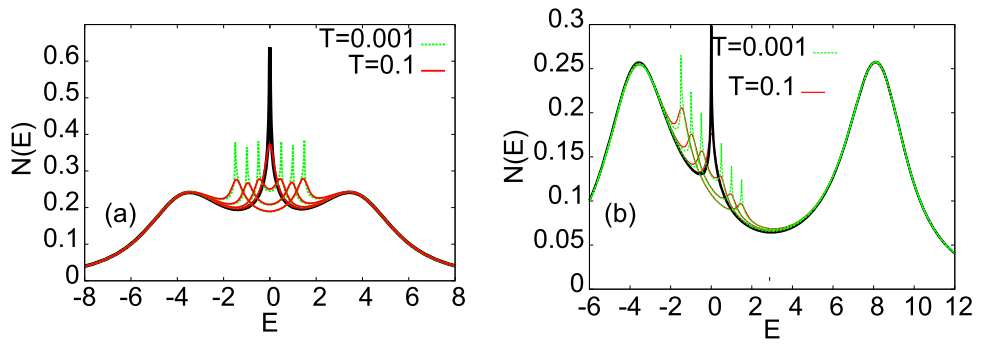

Figure 2. Density of states (DOS) for the particle-hole symmetric interacting quantum dot with $\varepsilon_d = -4$, $U = 8$ ($T_K \approx 0.061$) (a), and for $\varepsilon_d = -4$, $U = 12$ ($T_K \approx 0.026\,3$) (b), where the Kondo temperature, T_K, is calculated from the Haldane formula, equation (17). In both panels the DOS is given for two values of the system temperature, $T = 0.1$ and 0.001, and for a number of voltages V applied between left and right electrode. One observes the evolution of the Kondo peak with increasing bias. The black (solid) curve in both parts of the figure refers to $V = 0$ and $T = 0.001$, and the other curves to increasing values of V. Energies are given in units of $\Gamma_0 \equiv \Gamma_L$, here and in the following figures and their captions. Also in most formulas we set $k_B = 1$.

consistently from

$$\tilde{\varepsilon}_d = \varepsilon_d + \Sigma_1^T(\tilde{\varepsilon}_d) + \Sigma_2^T(\tilde{\varepsilon}_d). \tag{14}$$

The GF (11) has been shown to fulfil the unitarity limit, and to describe quantitatively correctly the Kondo effect [39] even in particle-hole symmetric systems in and out-of equilibrium.

3. Kondo effect in equilibrium and far from equilibrium

For illustrative purposes and in order to introduce the framework, we discuss in this section the properties of an interacting quantum dot between two normal electrodes, as illustrated in figure 1(a). We start the presentation of the results by showing the density of states (DOS) of the quantum dot, which is calculated as usual as $N(E) = -\sum_\sigma \mathrm{Im}\, G_\sigma^r(E)/\pi$ from the retarded Green function, in various regimes. From now on, we neglect the spin dependence of the couplings, and slightly change the notation: $\Gamma_\uparrow^L = \Gamma_\downarrow^L = \Gamma_L$, $\Gamma_\uparrow^R = \Gamma_\downarrow^R = \Gamma_R$. In addition, we measure all energies in units of $\Gamma_0 \equiv \Gamma_L$. The particle-hole symmetric case is of special importance as it is well known [39] that all previous attempts to use the EOM method failed in this case [58, 59]. The issue has been discussed extensively in the literature [43–45]; a critical comparison between EOM-based and other approximations has been presented very recently [60].

In figure 2 we present the DOS in the particle-hole symmetric situation with $\varepsilon_d = -4\Gamma_0$ and $U = 8\Gamma_0$. Both lower and upper Hubbard bands centered in energy around ε_d and $\varepsilon_d + U$ are clearly visible. At the same time, the Abrikosov–Suhl, sometimes also called Kondo resonance develops at the chemical potential.

The external bias shifts the chemical potentials of the leads $\mu_{L/R} = \mu \pm eV/2$ to new positions, and the Kondo peak splits into two with each resonance pinned to the chemical potential of the lead. In particular, figure 2 shows the evolution of the two peaks with temperature. At $T = 0.001\Gamma_0$, they are very sharp, while at $T = 0.1\Gamma_0$ they are reduced but still clearly visible. The changes of the Kondo resonance with bias and temperature are crucial to understand the behaviour of the thermally induced current and the (nonlinear) thermoelectric power as discussed in the next sections. At still higher temperatures (not shown) both Kondo peaks vanish altogether, and only lower and upper Hubbard bands survive. The Kondo resonance is due to spin flip processes on the dot while the Hubbard sub-bands are related to charge fluctuations. This explains the relative robustness of Hubbard sub-bands with increasing temperature, and the fragility of the Kondo correlations. However, voltage and temperature affect the Kondo resonance in a different way. While a voltage $eV > T_K$ leads to a splitting of the resonance in two sub-peaks with concomitant decrease of their maximum, the finite temperature only lowers the height of the peak and broadens it. All these features are well reproduced by the used decoupling scheme. Outside the particle-hole symmetric point, the voltage-split Kondo resonances are not symmetric anymore. This is mainly due to the closer proximity of one of the resonances to the lower Hubbard band. The individual resonances are pinned to the Fermi levels of the respective electrodes. This is well visible in figure 2(b), and also in figure 3(a).

We now add a thermal bias to one of the electrodes, with focus on the question of how the density of states evolves with temperature difference. We start with the split Kondo resonance as shown in figure 3(a). The temperature of the right lead is kept constant, at $T_R = T$, while we gradually increase the temperature of the left electrode, $T_L = T + \Delta T$. Panel (a) of figure 3 shows the voltage-split Kondo peaks for $\Delta T = 0$, for easy

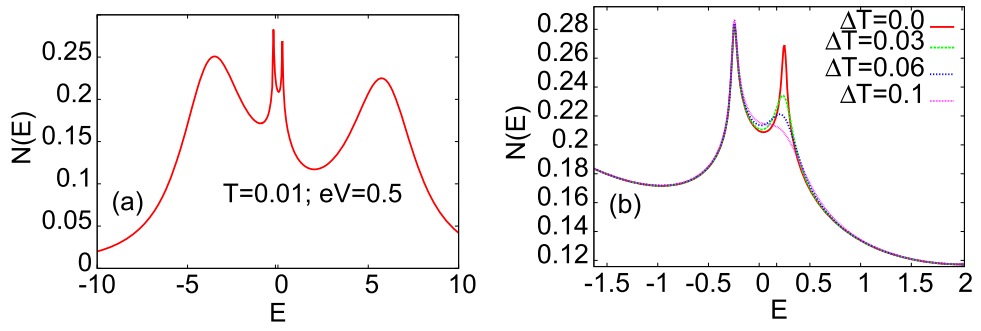

Figure 3. DOS of the quantum dot for the voltage $eV = 0.5$ applied between left and right electrode (a), showing two Kondo peaks pinned at the chemical potentials of the leads $\mu_{L/R} = \pm eV/2$. In panel (b) the evolution of the Kondo peaks with increase of temperature in the left lead by ΔT is illustrated. The other parameters are: $\varepsilon_d = -4$, $U = 10$, $T = 0.01$, and $\Gamma_R = 1$.

comparison, while panel (b) demonstrates the evolution of both peaks with increasing T_L. The peak pinned to the chemical potential of the left electrode (appearing at $E = \mu_L$) is strongly affected by the temperature bias, it broadens and vanishes with increasing temperature. One observes only small changes of the other Kondo peak. Thus under voltage and temperature bias the peaks' heights and widths depend mainly on the conditions (V, ΔT) at the electrode with the chemical potential to which it is pinned. For diminishing external voltage bias both peaks overlap in energy, and one observes a single feature in the density of states corresponding to the average temperature, $T_{\rm av} = (T_L + T_R)/2$, of the system.

4. Linear and nonlinear thermopower and the role of asymmetry

Nonlinear effects are expected to be important for many experiments on nano-devices [6, 15]. Hence in such cases alternative definitions of the thermoelectric coefficients are required. To start with, a suitable generalisation of the definition (1) of the Seebeck coefficient to nonlinear situations reads

$$S_n = -\left(\frac{V}{\Delta T}\right)_{I(\Delta T,V)=0}. \tag{15}$$

The traditional way to measure the Seebeck coefficient assumes the application of the temperature bias ΔT, and finding the voltage V such that the current across the device vanishes, $I(\Delta T, V) = 0$. In this formulation, the only source of nonlinearity is directly given by the value of ΔT, assumed to be large enough to preclude the linear expansion of the charge current $I(\Delta T, V)$ in first powers of V and ΔT.

On the contrary, when the linear expansion is valid, $V \to 0$ and $\Delta T \to 0$, we have $I(\Delta T, V) = L_{11}V + L_{12}\Delta T$, and the corresponding thermopower is given by the ratio of kinetic coefficients, $S = L_{12}/L_{11}$. Expanding equation (8) for small V and ΔT up to linear order, one finds an explicit expression for S.

Sometimes the definition (15) of the nonlinear Seebeck coefficient S_n is extended to the differential one, S_d, calculated formally for constant current flowing as a result of the external voltage V. This S_d measures the response of the system with current flow to a minute change in temperature difference. At a given applied external voltage V and temperature difference ΔT, S_d is hence defined [31, 61] as

$$S_d = -\left(\frac{\partial V}{\partial \Delta T}\right)_I = -\left(\frac{\partial I}{\partial \Delta T}\right)_V \Big/ \left(\frac{\partial I}{\partial V}\right)_{\Delta T}. \tag{16}$$

As argued earlier, S_d should be accessible experimentally [31] in appropriate ac circuits. In that paper, the response $(\partial I/\partial \Delta T)$ has been calculated under the additional assumption that, at a given external voltage, a very small temperature bias ΔT is applied to the system. The definition (16) is analogous to the differential conductance $G(V) = \partial I/\partial V$ often employed in the nonlinear regime.

Here we investigate the generalisation of S_d to arbitrary temperature differences and arbitrary bias as well as its comparison to S_n and S. Of course, for infinitesimally small ΔT and V all definitions are equivalent and lead to the same result, $S = S_n = S_d$. For arbitrary V and T but vanishingly small ΔT, the two nonlinear Seebeck coefficients are equal, $S_n = S_d$. However, for both a large ΔT and a large bias voltage V, they differ, with the relative values depending on the parameters (see below).

To gain some feeling about the relative values and the behaviour of the three, generally different Seebeck coefficients, we show in figure 4 the linear, S (where appropriate), as well as the nonlinear, S_n, and the differential, S_d, coefficients as calculated for the two-terminal device. The panels (a)–(c) in figure 4 illustrate their

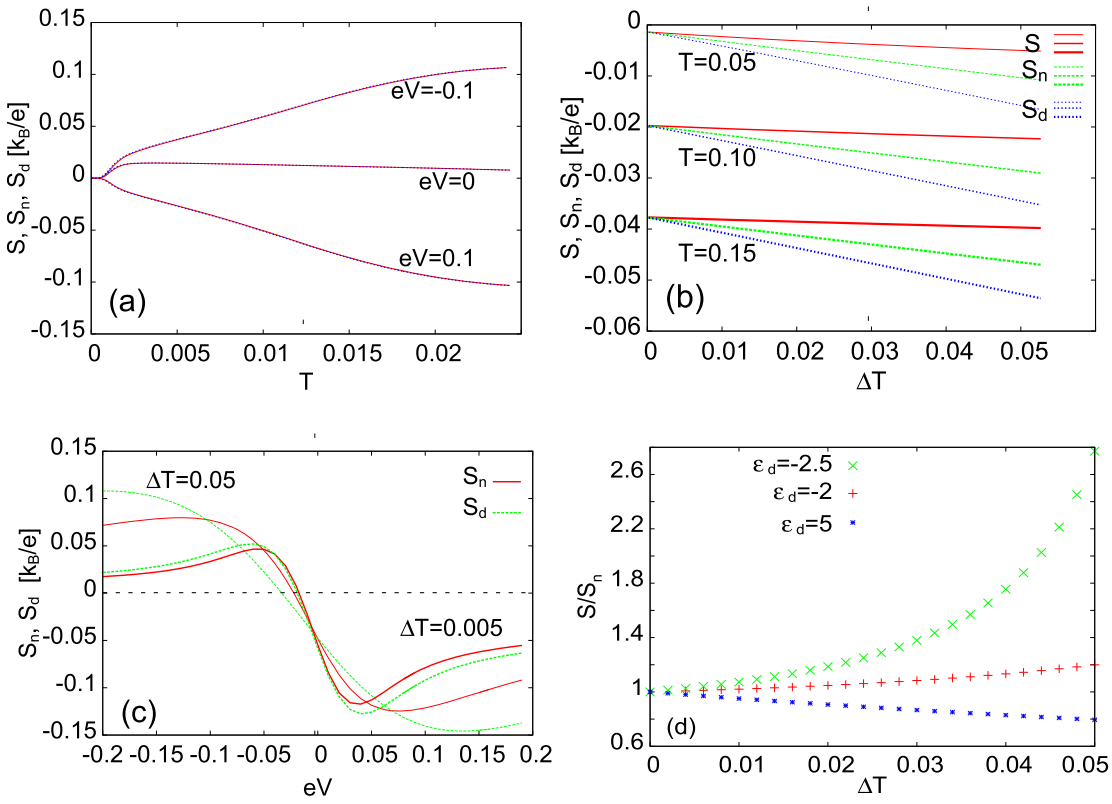

Figure 4. (a) The middle curve shows that all three Seebeck coefficients (linear, S, nonlinear, S_n, and differential, S_d) of the two-terminal device calculated for $V = 0$ and an infinitesimal value of ΔT agree with each other for all temperatures. The two other curves represent the nonlinear thermopowers $S_n = S_d$, calculated for two values of bias, $eV = -0.1$ and $eV = 0.1$. (b) Here we show the three thermopowers versus temperature difference ΔT between left and right electrodes, with $T_R = T$, $T_L = T + \Delta T$, calculated for the base temperatures $T = 0.05, 0.10$, and 0.15, and for $V = 0$. For large ΔT's strong nonlinearities are clearly visible, as well as apparent differences between the coefficients. (c) Voltage dependence of the nonlinear Seebeck coefficients S_n and S_d for two temperature differences, $\Delta T = 0.005$ and $\Delta T = 0.05$. (d) The ratio S/S_n depends on the system parameters. Here it is shown for $T = 0.1$, and $\varepsilon_d = -2.5, -2$, and 5. Other parameters are: $U = 8, \Gamma_0 \equiv \Gamma_L = \Gamma_R$. The results presented in panels (a)–(c) have been obtained for $\varepsilon_d = 5$.

dependence on temperature, temperature difference, and voltage. We assume $T_R = T$, $T_L = T + \Delta T$, $\mu_L = \mu + eV/2$, $\mu_R = \mu - eV/2$, and $U = 8\Gamma_0$, $\varepsilon_d = 5\Gamma_0$. For $U = 8\Gamma_0$ and $\varepsilon_d = -5\Gamma_0$, the Haldane formula for the Kondo temperature

$$T_K = \frac{\sqrt{U\Gamma_N}}{2} \exp\left[\frac{\pi\varepsilon_d(\varepsilon_d + U)}{\Gamma_N U}\right], \quad \Gamma_N = \frac{\Gamma_L + \Gamma_R}{2}, \tag{17}$$

leads to $T_K \approx 0.071\Gamma_0$.

Figure 4(a) illustrates the T-dependence of all Seebeck coefficients for three values of the voltage $eV = -0.1\Gamma_0, 0$, and $0.1\Gamma_0$, and for a very small temperature difference, $\Delta T \to 0$. The value $V = 0$ in fact denotes a very small voltage, $V \to 0$. For the actual calculations, we have used $\delta T = 10^{-9}\Gamma_0$, and to calculate the voltage derivative in (16) we have used $\delta V = 10^{-9}\Gamma_0$. All coefficients have the same value $S = S_n = S_d$ for $V \to 0$. For a relatively large value of V, the calculation of S is meaningless; the figure shows that independent of T and for both values of V one has $S_n = S_d$ (since the applied temperature difference is infinitesimal).

The situation is different if ΔT is finite. The results for $V = 0$ are presented in figure 4(b); it is apparent that all coefficients assume different values, except for very small ΔT. The differences increase with increasing ΔT, with S_d lying below S_n (and S_n below S) for all T and a given set of parameters.

For finite voltages the relative order of S_n and S_d may be different, as is visible from panel (c) of the figure. The Seebeck coefficient S_n provides a generalisation of the standard definition to the nonlinear regime, while the differential one, S_d, characterises the response to a minute temperature change of the voltage biased system. The data presented in figure 4(c) have been obtained for $T = 0.01\Gamma_0$, and the two values $\Delta T = 0.005\Gamma_0$ and $0.05\Gamma_0$. For small temperature bias the curves corresponding to S_n and S_d are rather close to each other. However, for larger ΔT the nonlinear dependence of the Fermi functions and the on-dot density of states on V and ΔT lead to various contributions to both S_n and S_d.

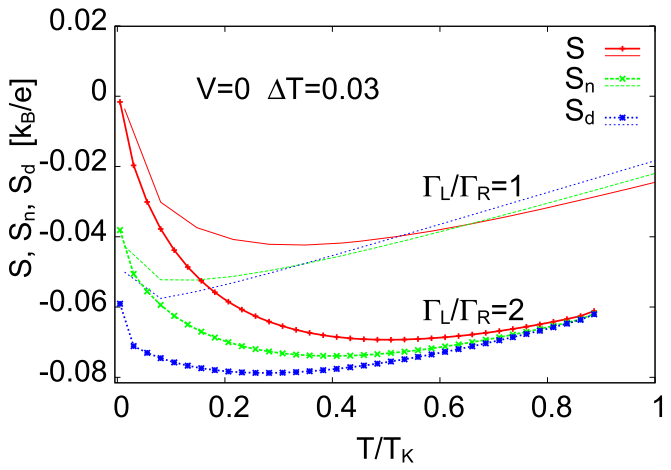

Figure 5. The anisotropy of the couplings $\Gamma_R/\Gamma_L \neq 1$ results in increased absolute values of the Seebeck coefficients. We show all three coefficients, albeit the temperature difference $\Delta T = 0.03$ is slightly beyond the validity of the linear approximation. Other parameters of the model read: $U = 8, \varepsilon_d = -5$. The Kondo temperature is $T_K \approx 0.004$ for the symmetric case, $\Gamma_R/\Gamma_L = 1$, and ≈ 0.034 for $\Gamma_R/\Gamma_L = 2$.

It has to be underlined that S can be smaller or larger than S_n, depending on the system parameters. For example, for $\varepsilon_d = -2.5\Gamma_0$, $T = 0.1\Gamma_0$, and other parameters as in figure 4(d), we have $|S| > |S_n|$, with the difference increasing with ΔT. It is also apparent that for $\varepsilon_d = 5\Gamma_0$ the ratio is smaller than one, i.e. for these parameters the linear thermopower happens to be smaller than the nonlinear one.

The non-zero value of both Seebeck coefficients S_n and S_d for $V = 0$ in figure 4(c) can be understood by taking into account the lack of particle-hole symmetry, $2\varepsilon_d + U \neq 0$, for the set of parameters used. For these parameters the density of states is similar to that shown in panel (b) of figure 2. The differences between the curves $S_n(V)$ and $S_d(V)$ for the same ΔT are of the same character as those observed in figure 4(b), while the global similarities between the two sets of curves calculated for $\Delta T = 0.005\Gamma_0$ and $\Delta T = 0.05\Gamma_0$ can be traced back to a larger contribution to $(\partial I/\partial \Delta T)$ obtained from equation (8):

$$\left(\frac{\partial I}{\partial \Delta T}\right) \approx -\frac{2e}{\hbar}\sum_\sigma \tilde{\Gamma}_\sigma \int \frac{\mathrm{d}E}{2}\left\{[f_L(E,\,T) - f_R(E,\,T)]\left(\frac{\partial N(E,\,T,\,\Delta T)}{\partial \Delta T}\right)\right.$$
$$\left. - N(E,\,T,\,\Delta T)\left(-\frac{\partial f_L(E)}{\partial \Delta T}\right)\right\} + O((\Delta T)^2) + \cdots \tag{18}$$

Note that the difference

$$D(V) = [f_L(E,\,T) - f_R(E,\,T)] = -D(-V) \tag{19}$$

is an odd function of the voltage, which implies that the resulting curves are nearly anti-symmetric with respect to $V = 0$ (and that the ordinates are equal, $S_n(0) \approx S_d(0)$). The smaller contribution proportional to $(-\partial f_L(E)/\partial \Delta T)$ depends on V in a non-universal way. This causes the crossing of two coefficients at various voltages and for ΔT well beyond the validity of the linear approximation.

We remark that the differential Seebeck coefficient, S_d, has been analysed in [31, 61]; in particular, the authors claim that S_d allows for a better understanding of decoherence processes at finite voltage. Indeed, as observed in figure 3(b), the decoherence processes at finite voltage V are mainly induced by the increase of temperature at one of the electrodes. These processes are most effective at energies around the chemical potential of the hotter electrode. It follows from our calculations of S_d, which is typically larger than S, that measuring the thermopower under a finite voltage and sensing the temperature at the same time may be challenging, as the current flow (over-)heats the system. In fact, overheating of a metallic quantum dot has been observed in recent measurements of the thermovoltage in a two-terminal device [62], despite the open circuit ($I = 0$) condition.

We note that the asymmetry of the couplings $\Gamma_L \neq \Gamma_R$ also affects the Seebeck coefficients. To see this, we assume $V = 0$ and a relatively small temperature difference $\Delta T = 0.03\Gamma_0$. Figure 5 shows S, S_n, and S_d, calculated for symmetric coupling (thin lines) as well as for an asymmetric system with $\Gamma_R/\Gamma_L = 2$ (thick lines). Interestingly, the largest decrease of the Seebeck coefficient is observed at low temperatures, well below the Kondo temperature, in agreement with recent findings [61] based on the non-crossing approximation. The Seebeck coefficient has a minimum at temperatures below T_K, and the minimum is lower for the asymmetric

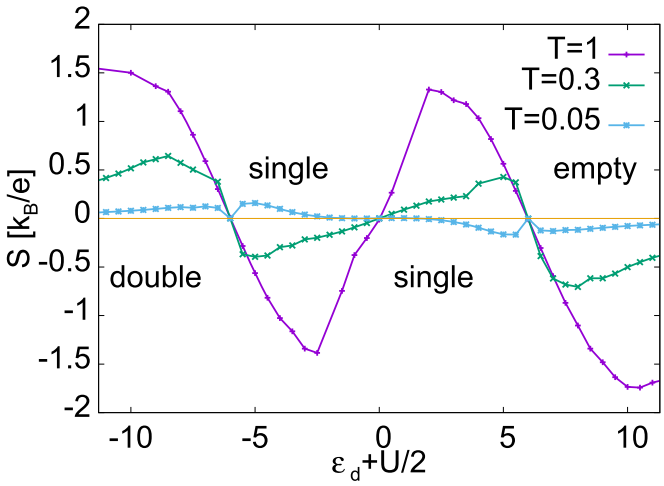

Figure 6. Linear Seebeck coefficient (S), calculated for three temperatures $T = 1, 0.3$, and 0.05, versus $\varepsilon_d + U/2$ which measures the distance from the particle-hole symmetric point. The interaction parameter is $U = 12$, and $\Gamma_L = \Gamma_R$. The indicated occupancy of the level ε_d depends on the gate voltage.

coupling. The asymmetry of the couplings is an important experimental observation [63], and should be taken into account in any calculation comparing with experiment [64].

The experiment mentioned above [62] has shown the usefulness of the nonlinear Seebeck coefficient for the analysis of the experimental data. The authors have directly measured the thermovoltage $V_{\rm th}$ of a two-terminal device, similar to that shown in figure 1(a), however, for a sizable metallic island. In order to compare experimental data with theory, $V_{\rm th}$ was calculated as $S \cdot \Delta T$: notably, the agreement can be improved (details depending on parameters) when using the nonlinear expression [62], i.e. the calculated S_n instead of S. The remaining disagreement is likely due to heating. In this context, it may also be useful to employ the differential coefficient, S_d. However, a detailed quantitative comparison with experimental results is beyond the scope of this paper, since, *inter alia*, the model investigated here likely is too simplified compared to the metallic islands actually studied.

Our theory also allows to explain the results shown in figure 4(a) of a recent experimental paper [29], albeit with a notable exception. These authors have found 'striking' sign changes of the Seebeck coefficients, in addition to the standard sign change at the particle-hole symmetric point. These sign changes depend on the spin configuration of the quantum dot and are observed with increasing temperature. In the experiment [29], S in fact changes sign at three values of the gate voltage, with one of them at the particle-hole symmetric point. Two other gate voltages at which sign changes appear are related to consecutive energy levels crossing the chemical potential.

In our theory for the single-level quantum dot, the sign change is observed when one of the resonance levels ε_d or $\varepsilon_d + U$ crosses the Fermi level in response to the gate voltage. In order to describe this effect, we have calculated the linear Seebeck coefficient for $U = 12\Gamma_0$, and for three different temperatures, see figure 6. One sees that the Seebeck coefficient vanishes not only at the particle-hole symmetric point, $\varepsilon_d + U/2 = 0$, but also at the points $\varepsilon_d + U/2 = -6\Gamma_0$ and $\varepsilon_d + U/2 = 6\Gamma_0$. In the range $\varepsilon_d + U/2 > -6\Gamma_0$, S is positive for low T but negative for elevated temperatures. For the considered value of $U = 12\Gamma_0$, and for a gate voltage such that $\varepsilon_d + U/2 = -6\Gamma_0$, the doubly occupied level $\varepsilon_d + U$ just crosses the chemical potential (located at zero energy) from below. This implies that at this gate voltage the system crosses over from double to single occupancy. A similar situation is observed to the left of $\varepsilon_d + U/2 = 6\Gamma_0$, when the level ε_d crosses the Fermi energy and the occupancy changes from single occupation to empty with increasing $\varepsilon_d + U/2$ from below to above $6\Gamma_0$.

The vanishing of the high temperature thermopower at these two points in our approach results from the perfect symmetry of the dot density of states around the Fermi energy for the corresponding two gate voltages. At very low temperature, the Kondo effect sets in and we are getting very deep minima when ε_d or $\varepsilon_d + U$ cross the chemical potential, while experiment shows a local maximum of the thermopower at these points for $T < T_K$. We emphasise that the typical asymmetry of the Kondo peak outside the particle-hole symmetry point is well reproduced by the present approach. The experimental data in figure 4(a) in [29], on the other hand, seem to show only positive (or negative), i.e. finite values of S around those special points at the lowest temperatures, with an apparent maximum (minimum) at the gate voltage where the theoretical Seebeck coefficient has a dip (peak).

In this context, we also wish to mention the experimental results presented by Svilans *et al* [65], which for zero magnetic field are essentially very similar to our findings (figure 6). The experimental results are analysed theoretically in [66] with focus on the field dependence, employing the numerical renormalisation group (NRG) method. While this technique is numerically exact, it is limited to linear response. In particular, the NRG method provides a maximum of S, in agreement with experiment, where our elaborated EOM technique predicts a dip. Seemingly, the NRG characterises the Kondo state better than the EOM method.

5. Three-terminal thermoelectric heat engine: the role of strong Coulomb interactions

As already noted, a thermoelectric device can serve as waste heat to electricity converter. Since energy harvesting is an important issue at large and small scales, its proper understanding may have important scientific and societal implications. As discussed in the Introduction, the figure of merit, ZT, ceases to be a good quality indicator in nanostructures [13, 15], and both the power and the efficiency are required. The quantities of interest are the maximum power, and the efficiency at maximum power. As it turns out the interactions between electrons strongly modify all transport characteristics. In the present model, the linear response calculations generally lead to lower values of η/η_C than those obtained from the fully self-consistent results, to be described in the following. However, in both cases the interactions tend to diminish the maximal power and the efficiency.

The focus of this section is on the effects of strong interactions between the on-dot electrons on the performance characteristics of the three-terminal heat engine shown in figure 1(b). For the non-interacting case but well outside equilibrium, such a device has been studied earlier [28, 38]. A more recent extension takes screening effects into account, treating the interactions within a mean-field approximation [37]. The main conclusion was that albeit the screening modifies the parameters at which the engine is optimal, it does neither change the maximal power nor the efficiency at maximum power. A similar heat engine has also been optimised with respect to the transmission function [67].

In particular, we have found [37] that the three-terminal heat engine at optimised conditions attains an efficiency slightly above 0.2 in units of the Carnot efficiency, and that this value is roughly the same as the one without screening effects. The optimisation involved the effective coupling between the dots and the leads, $\Gamma/T_{\rm av}$, the temperature difference between the electrodes, $\Delta T/T_{\rm av}$, and the load voltage, V; $T_{\rm av}$ denotes the average temperature of the system. (The coupling Γ introduced here refers to the symmetric case with $\Gamma_L = \Gamma_R = \Gamma_H \equiv \Gamma$ [37]). The calculations have shown that the optimal coupling, i.e. the one leading to the maximal power if other parameters remain fixed, is of the order of the average temperature, $\Gamma/T_{\rm av} \approx 1$. The efficiency has been found to depend rather weakly, and the power strongly on the temperature difference ΔT between the hot (H), $T_H = T + \Delta T$, and the two cold (R, L) electrodes, $T_R = T_L = T$.

Here we shall pursue the analysis assuming nonlinear working conditions and taking strong interactions into account. In particular, the calculations include the Kondo regime. To this end, we use the general expressions (3) for the charge and (4) for the heat current flowing out of the λ lead, energy conservation, and the general expression (11) for the on-dot Green function. From the charge current flowing from the left to the right electrode, and the heat current flowing from the hot to the cold electrodes, we calculate the performance of the engine as quantified by the maximum power P, and the efficiency η at maximum power.

In order to demonstrate the effect of the Coulomb interaction on the performance of the engine, we show in figure 7 the efficiency η versus power P. The efficiency is measured in units of the Carnot efficiency, $\eta_C = \Delta T/T_H = 0.4$, and the power is normalized by $(k_{\rm B}T_{\rm av})^2$. The plot shown in panel (a) has been obtained by calculating the heat and charge currents as well as the optimal voltage (and the power) for a given difference of the dot's energy levels, $\Delta E = \varepsilon_R - \varepsilon_L$, where ε_R (ε_L) refers to the energy level of the right (left) dot, see figure 1. Note that for appropriate values of ε_R (ε_L) and low temperature, the respective dot may show Kondo behaviour. This has an important effect on the η–P plot.

In panel (a) of figure 7 one sees that the $U = 0$ curve essentially encompasses all curves obtained for the interacting case. Coulomb interactions generally suppress the performance characteristics—at least so under the assumptions of the present approach, including the wide-band approximation. The temperature of all electrodes are such that this system (figure 7(a)) is always outside the Kondo regime.

To illustrate the behaviour of an engine working in the Kondo regime, we show in figure 7(b) a similar plot, but obtained for a two-terminal system and a much lower value of the average temperature. For the interaction $U = 8\Gamma_0$, and temperatures $T_L = 0.15\Gamma_0$, $T_R = 0.25\Gamma_0$, the dot enters the Kondo regime for a range of gate voltages (or ε_d). The Kondo effect results in the appearance of the new performance branch on the η–P plane. As visible in panel (b) of the figure, this region is characterised by efficiencies and powers lower than those outside the Kondo regime.

The results shown in figure 7 have been obtained under the assumption that the couplings to the leads equals the average temperature, $\Gamma = T_{\rm av}$, the value which has been found to be optimal (i.e. leading to the maximal

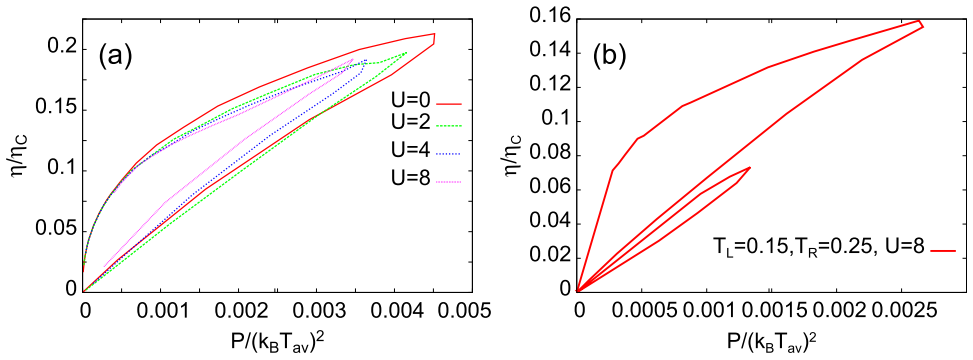

Figure 7. Panel (a) shows efficiency versus power for the three-terminal quantum dot engine, assuming optimal values of the couplings: $\Gamma_L = \Gamma_R = \Gamma_H \equiv \Gamma = T_{\rm av}$, with $\Delta T = 0.5$, $T_L = T_R = T = 0.75$, $T_H = T + \Delta T = 1.25$, $T_{\rm av} = T + \Delta T/2$, and a few values of the Coulomb interaction parameters U. Panel (b) shows the efficiency versus power plot for a two-terminal system. For $U = 8$ and a range of values of the dot energies ε_d, the Kondo effect is observed at the considered temperatures. The Kondo effect results in the second (lower) branch on the η–P plane. In the Kondo region the performance of the system as a heat engine does not exceed that in the other region.

power) for the non-interacting system. Analogous to [37], we change the dots' energy levels, thereby varying the difference $\Delta E = \varepsilon_R - \varepsilon_L$, and calculate the power and efficiency for each ΔE for the optimised value of the load voltage V. The curves in figure 7 are thus parametrised by ΔE.

Regarding the experimental situation, very recently a three-terminal two-quantum-dot system identical to the three-terminal system studied here has been found [68] to generate a power of 0.13 fW, its efficiency being estimated to be larger than $\eta \approx 0.1\eta_C$. To find the actual values of the device power, we need the width of the resonance level, Γ. Assuming $\Gamma = 0.15$ meV (which is the average value of those mentioned in figure 4 of [68]), we find that the maximal power in figure 7(a) equals 3.92 fW. The corresponding estimate of the power at the efficiency $\eta/\eta_C = 0.1$ gives $P = 0.44$ fW, in good agreement with the experimental value, taking into account the uncertainty in estimating Γ, its non-optimal value in the actual experiment, and a possible asymmetry of the couplings. In fact, the maximal efficiency we obtain, for optimised parameters, is slightly above 0.2 of the Carnot value.

6. Summary and conclusions

We have studied the thermoelectric transport properties of two- and three-terminal systems with quantum dots, paying attention to strong interactions of electrons on the dot(s) and far-from-equilibrium conditions. As theoretical tool, we have used the suitably generalised equation of motion technique. We have shown that the method is able to capture the Kondo resonance even for a system with particle-hole symmetry. The voltage across the system splits the resonance. Interestingly, the increase of the temperature of one of the electrodes affects the Kondo resonance pinned to the chemical potential of that electrode. This adds to the discussion of decoherence effects in non-equilibrium conditions. It turns out that the decoherence mainly takes place at energies close to the chemical potential of the electrode with temperature higher than the Kondo temperature.

Of particular importance is the nonlinear regime at large external voltage bias V and large temperature difference ΔT, since the linear approximation is hardly ever valid in nanostructures. This has been again confirmed here, and is visible as the detrimental effect of strong correlations on the performance of the three-terminal optimised heat engine. Calculating the maximum power P and the efficiency η of the optimised device for various interactions U, we have observed that except at very low temperatures the curves calculated for $U \neq 0$ are encompassed by the curve obtained for the non-interacting system. Obviously the filtering properties of the quantum dots are affected by the interactions which broaden or split the density of states, rendering the filter less effective. This agrees with previous attempts at optimising heat engines by engineering the transmission function [23, 67]. On the other hand, strong interactions are responsible for the second leaf on the efficiency versus power plane, visible in figure 7(b). This special feature appears at low temperatures when the system enters the Kondo regime, albeit for a relatively small range of gate voltages. However, the maximum values of P and η are well below those on the main branch.

The generalisation of the standard linear-response Seebeck coefficient, S, to the strongly nonlinear regime has led us to define two coefficients, S_n and S_d, cf equations (15) and (16). Both are, in principle, valid for arbitrary values of V and ΔT, albeit the first coefficient, S_n, is easier to handle in systems with zero external voltage but arbitrarily large temperature difference between a given pair of electrodes. The second, called differential Seebeck coefficient, has been applied earlier [31, 61] to systems with finite current flow and a small

temperature difference. It has been generalized and studied here for arbitrary ΔT in the presence of an external voltage bias V. Interestingly, the asymmetry of the couplings to the external leads has a qualitatively similar influence on both Seebeck coefficients. They develop a minimum for temperatures well below the Kondo temperature. The observed quantitative differences between S_n and S_d are expected to be important for temperature sensing by means of thermopower measurements [69].

The approach developed in this work has significantly enhanced the understanding of non-equilibrium thermal transport through quantum-dot based devices, in particular, it has the potential to describe the existing as well as future experiments on such systems.

Acknowledgments

The work reported here has been supported by the M Curie-Skłodowska University, National Science Center grant DEC-2017/27/B/ST3/01911 (Poland), the Deutsche Forschungsgemeinschaft (DFG, project no. 107745057, TRR 80), and the University of Augsburg.

ORCID iDs

Ulrich Eckern https://orcid.org/0000-0001-8917-9083
Karol I Wysokiński https://orcid.org/0000-0002-5366-4455

References

[1] Yang J H and Caillat T 2006 Thermoelectric materials for space and automotive power generation *MRS Bull.* **31** 224
[2] Chu S and Majumdar A 2012 Opportunities and challenges for a sustainable energy future *Nature* **488** 294
[3] Whitney R S, Sánchez R and Splettstoesser J 2018 Quantum thermodynamics of nanoscale thermoelectrics and electronic devices *Thermodynamics in the Quantum Regime, Fundamental Theories of Physics* ed F Binder *et al* vol 195 (Cham: Springer) p 175
[4] Ren Z, Lan Y and Zhang Q (ed) 2018 *Advanced Termoelectrics: Materials, Contacts, Devices, and Systems* (Boca Baton, FL: CRC Press)
[5] Gooth J, Schierning G, Felser C and Nielsch K 2018 Quantum materials for thermoelectricity *MRS Bull.* **43** 187
[6] Benenti G, Casati G, Saito K and Whitney R S 2017 Fundamental aspects of steady-state conversion of heat to work at the nanoscale *Phys. Rep.* **694** 1
[7] Zimbovskaya N A and Pederson M R 2011 Electron transport through molecular junctions *Phys. Rep.* **509** 1
[8] Russ B, Glaudell A, Urban J J, Chabinyc M L and Segalman R A 2016 Organic thermoelectric materials for energy harvesting and temperature control *Nat. Rev. Mater.* **1** 16050
[9] Josefsson M, Svilans A, Burke A M, Hoffmann E A, Fahlvik S, Thelander C, Leijnse M and Linke H 2018 A quantum dot heat engine operating close to the thermodynamic efficiency limits *Nat. Nanotechnol.* **13** 920
[10] Costi T A and Zlatić V 2010 Thermoelectric transport through strongly correlated quantum dots *Phys. Rev.* B **81** 235127
[11] Mazza F, Bosisio R, Benenti G, Giovannetti V, Fazio R and Taddei F 2014 Thermoelectric efficiency of three-terminal quantum thermal machines *New J. Phys.* **16** 085001
[12] Michałek G, Urbaniak M, Bułka B R, Domański T and Wysokiński K I 2016 Local and nonlocal thermopower in three-terminal nanostructures *Phys. Rev.* B **93** 235440
[13] Muralidharan B and Grifoni M 2012 Performance analysis of an interacting quantum dot thermoelectric setup *Phys. Rev.* B **85** 155423
[14] Whitney R S 2013 Nonlinear thermoelectricity in point contacts at pinch off: a catastrophe aids cooling *Phys. Rev.* B **88** 064302
[15] Wysokiński K I, Domański T, Szukiewicz B, Michałek G and Bułka B R 2016 Quantum transport in hybrid nanostructures *Symmetry, Spin Dynamics and the Properties Of Nanostructures* ed V Dugaev *et al* (Singapore: World Scientific)
[16] Finch C M, Garcia-Suarez V M and Lambert C J 2009 Giant thermopower and figure of merit in single-molecule devices *Phys. Rev.* B **79** 033405
[17] Meair J and Jacquod P 2013 Scattering theory of non-linear thermoelectricity in quantum coherent conductors *J. Phys.: Condens. Matter* **25** 082201
[18] Szukiewicz B and Wysokiński K I 2015 Quantum dot as spin current generator and energy harvester *Eur. Phys. J.* B **88** 112
[19] Kleeorin Y, Thierschmann H, Buhmann H, Georges A, Molenkamp L W and Meir Y 2019 Measuring the Entropy of a Mesoscopic System via thermoelectric transport arXiv:1904.08948
[20] Heremans J P, Thrush Ch M and Morelli D T 2004 Thermopower enhancement in lead telluride nanostructures *Phys. Rev.* B **70** 115334
[21] Mahan G D and Sofo J O 1996 The best thermoelectric *Proc. Natl Acad. Sci.* **93** 7436
[22] Heremans J P, Wiendlocha B and Chamoire A M 2012 Resonant levels in bulk thermoelectric semiconductors *Energy Environ. Sci.* **5** 5510
[23] Hershfield S, Muttalib K A and Nartowt B J 2013 Nonlinear thermoelectric transport: a class of nanodevices for high efficiency and large power output *Phys. Rev.* B **88** 085426
[24] Balseiro C A, Usaj G and Sánchez M J 2010 Out of equilibrium transport through an Anderson impurity: probing scaling laws within the equation of motion approach *J. Phys.: Condens. Matter* **22** 425602
[25] Dutt P and Le Hur K 2013 Strongly correlated thermoelectric transport beyond linear response *Phys. Rev.* B **88** 235133
[26] Lopez R and Sánchez D 2013 Nonlinear heat transport in mesoscopic conductors: rectification, Peltier effect, and Wiedemann–Franz law *Phys. Rev.* B **88** 045129
[27] Azema J, Lombardo P and Daré A-M 2014 Conditions for requiring non-linear thermoelectric transport theory in nanodevices *Phys. Rev.* B **90** 205437
[28] Jordan A N, Sothmann B, Sánchez R and Büttiker M 2013 Powerful and efficient energy harvester with resonant tunneling quantum dots *Phys. Rev.* B **87** 075312

[29] Dutta B, Majidi D, García Corral A, Erdman P A, Florens S, Costi T A, Courtois H and Winkelmann C B 2019 Direct probe of the Seebeck coefficient in a Kondo-correlated single-quantum-dot transistor *Nano Lett.* **19** 506
[30] Sánchez D and Lopez R 2016 Nonlinear phenomena in quantum thermoelectrics and heat *C. R. Phys.* **17** 1060
[31] Dorda A, Ganahl M, Andergassen S, von der Linden W and Arrigoni E 2016 Thermoelectric response of a correlated impurity in the nonequilibrium Kondo regime *Phys. Rev.* B **94** 245125
[32] Glazman L I and Raikh M E 1988 Resonant Kondo transparency of a barrier with quasilocal impurity states *Pisma Zh. Eksp. Teor. Fiz.* **47** 378 [1988 *JETP Lett.* **47** 452 (Engl. Transl.)]
[33] Ng T K and Lee P A 1988 On-Site Coulomb repulsion and resonant tunneling *Phys. Rev. Lett.* **61** 1768
[34] Goldhaber-Gordon D, Shtrikman H, Mahalu D, Abush-Maggder D, Meirav U and Kastner M A 1998 Kondo effect in a single-electron transistor *Nature* **391** 156
[35] Cronenwett S M, Oosterkamp T H and Kouwenhoven L P 1998 A tunable Kondo effect in quantum dots *Science* **281** 540
[36] Schmid J, Weis J, Eberl K and von Klitzing K 1998 A quantum dot in the limit of strong coupling to reservoirs *Physica* B **256-258** 182
[37] Szukiewicz B, Eckern U and Wysokiński K I 2016 Optimisation of a three-terminal non-linear heat nano-engine *New J. Phys.* **18** 023050
[38] Donsa S, Andergassen S and Held K 2014 Double quantum dot as a minimal thermoelectric generator *Phys. Rev.* B **89** 125103
[39] Lavagna M 2015 Transport through an interacting quantum dot driven out-of-equilibrium *J. Phys.: Conf. Ser.* **592** 012141
[40] Zubarev D N 1960 Double-time Green functions in statistical physics *Usp. Fiz. Nauk.* **71** 71 [1960 *Sov. Phys. Usp.* **3** 320 (Engl. Transl.)]
[41] Haug H and Jauho A-P 2008 *Quantum Kinetics in Transport and Optics of Semiconductors* (Berlin: Springer)
[42] Anderson P W 1961 Localized magnetic states in metals *Phys. Rev.* **124** 41
[43] Appelbaum J A and Penn D R 1969 Localized correlations in narrow conduction bands. I *Phys. Rev.* **188** 874
Theumann A 1969 Self-consistent solution of the Anderson model *Phys. Rev.* **178** 978
Mamada H and Takano F 1970 Self-consistent treatment of Anderson model and magnetic susceptibility *Prog. Theor. Phys.* **43** 1458
Poo G S 1975 Magnetic field effects in the Anderson model of dilute magnetic alloys. I. self-consistent solution *Phys. Rev.* B **11** 4606
[44] Lacroix C 1981 Density of states for the Anderson model *J. Phys. F: Met. Phys.* **11** 2389
Lacroix C 1982 Density of states for the asymmetric Anderson model *J. Appl. Phys.* **53** 2131
[45] Kashcheyevs V, Aharony A and Entin-Wohlman O 2006 Applicability of the equations-of-motion technique for quantum dots *Phys. Rev.* B **73** 125338
[46] Langreth D C 1976 Linear and nonlinear response theory with applications *Linear and Non-linear Electron Transport in Solids* ed J T Devreese and V E van Doren (New York: Plenum) p 3
[47] Wysokiński M M 2012 Thermoelectric effect in the normal conductor-superconductor junction: a BTK approach *Acta Phys. Pol.* A **122** 758
[48] Wysokiński M M and Spałek J 2013 Seebeck effect in the graphene-superconductor junction *J. Appl. Phys.* **113** 163905
[49] Wysokiński M M 2014 Temperature dependence of the zero-bias conductance in the graphene NIS junction *Acta Phys. Pol.* A **126** A36
[50] Polkovnikov A 2002 Kondo effect in d-wave superconductors *Phys. Rev.* B **65** 064503
[51] Ng T-K 1996 ac response in the nonequilibrium Anderson impurity model *Phys. Rev. Lett.* **76** 487
[52] Niu C, Lin D L and Lin T-H 1999 equation of motion for nonequilibrium Green functions *J. Phys.: Condens. Matter* **11** 1511
[53] Dias da Silva L G G V, Lewenkopf C H, Vernek E, Ferreira G J and Ullo S E 2017 Conductance and Kondo interference beyond proportional coupling *Phys. Rev. Lett.* **119** 116801
[54] Meir Y and Wingreen N S 1992 Landauer formula for the current through an interacting electron region *Phys. Rev. Lett.* **68** 2512
Wingreen N S and Meir Y 1994 Anderson model out of equilibrium: noncrossing-approximation approach to transport through a quantum dot *Phys. Rev.* B **49** 11040
[55] Hirsch J E and Fye R M 1986 Monte Carlo method for magnetic impurities in metals *Phys. Rev. Lett.* **56** 2521
[56] Bulla R, Costi T A and Pruschke T 2008 Numerical renormalization group method for quantum impurity systems *Rev. Mod. Phys.* **80** 395
[57] Van Roermund R, Shiau S-Y and Lavagna M 2010 Anderson model out of equilibrium: decoherence effects in transport through a quantum dot *Phys. Rev.* B **81** 165115
[58] Domański T, Donabidowicz A and Wysokiński K I 2008 Meservey–Tedrow–Fulde effect in a quantum dot embedded between metallic and superconducting electrodes *Phys. Rev.* B **78** 144515
[59] Michałek G, Bułka B R, Domański T and Wysokiński K I 2013 Interplay between direct and crossed Andreev reflections in hybrid nanostructures *Phys. Rev.* B **88** 155425
[60] de Souza Melo B M, Dias da Silva L G G V, Rocha A R and Lewenkopf C H 2020 Quantitative comparison of Anderson impurity solvers applied to transport in quantum dots *J. Phys.: Condens. Matter* **32** 095602
[61] Daroca D P, Roura-Bas P and Aligia A A 2018 Enhancing the non-linear thermoelectric response of a correlated quantum dot in the Kondo regime by asymmetrical coupling to the leads *Phys. Rev.* B **97** 165433
[62] Erdman P A, Peltonen J T, Bhandari B, Dutta B, Courtois H, Fazio R, Taddei F and Pekola J P 2019 Nonlinear thermovoltage in a single-electron transistor *Phys. Rev.* B **99** 165405
[63] Delagrange R, Basset J, Bouchiat H and Deblock R 2018 Emission noise and high frequency cut-off of the Kondo effect in a quantum dot *Phys. Rev.* B **97** 041412
[64] Crépieux A, Sahoo S, Duong T Q, Zamoum R and Lavagna M 2018 Emission noise in an interacting quantum dot: role of inelastic scattering and asymmetric coupling to the reservoirs *Phys. Rev. Lett.* **120** 107702
[65] Svilans A, Josefsson M, Burke A M, Fahlvik S, Thelander C, Linke H and Leijnse M 2018 Thermoelectric characterization of the Kondo resonance in nanowire quantum dots *Phys. Rev. Lett.* **121** 206801
[66] Costi T A 2019 Magnetic field dependence of the thermopower of Kondo-correlated quantum dots *Phys. Rev.* B **100** 161106(R)
[67] Schiegg C H, Dzierzawa M and Eckern U 2017 Implementation of transmission functions for an optimised three-terminal quantum dot heat engine *J. Phys.: Condens. Matter* **29** 085303
[68] Jaliel G, Puddy R K, Sánchez R, Jordan A N, Sothmann B, Farrer I, Griffiths J P, Ritchie D A and Smith C G 2019 Experimental realization of a quantum dot energy harvester *Phys. Rev. Lett.* **123** 117701
[69] Kleinbaum E I and Lyon S A 2018 Thermopower-based hot electron thermometry of helium surface states at 1.6 K *Phys. Rev. Lett.* **121** 236801